

# Short Papers

## Modeling and Analysis of Crosstalk Noise in Coupled *RLC* Interconnects

Kanak Agarwal, Dennis Sylvester, and David Blaauw

**Abstract**—At current operating frequencies, inductive-coupling effects can be significant and should be included for accurate crosstalk-noise analysis. In this paper, an analytical framework to model crosstalk noise in coupled *RLC* interconnects is presented. The proposed model is based on transmission-line theory and captures high-frequency effects in on-chip interconnects. The new model is generic in nature and can be applied to asymmetric driver-and-line configurations for aggressor and victim wires. The model is compared against SPICE simulations and is shown to capture both the waveform shape and peak noise accurately. Over a large set of random test cases, the average error in noise-peak estimation is approximately 6.5%. A key feature of the new model is that its derivation and form enables physical insight into the total coupling-noise-waveform shape and its dependence on relevant physical-design parameters. Due to its simplicity and physical nature, the proposed model can be applied to investigate the impact of various physical-design optimizations (e.g., wire sizing and spacing, shield insertion) on total *RLC* coupled noise. The effectiveness of various existing noise-reduction techniques in the presence of mutual-inductance coupling is studied here. The obtained results indicate that common (capacitive) noise-avoidance techniques can behave quite differently when both capacitive and inductive coupling are considered together.

**Index Terms**—Coupling, crosstalk noise, inductance, integrated circuit interconnect, mutual inductance, signal integrity, transmission lines.

### I. INTRODUCTION

On-chip inductance has become significant in designs with gigahertz clock frequencies [1], [2]. Due to this increased importance of inductive effects in on-chip interconnects, traditional lumped and distributed *RC* models of interconnects are no longer accurate as they result in substantial errors in predicting delay and crosstalk [3], [4]. There has been recent work to include the impact of self-inductance during gate [5], [6] and interconnect delay prediction [7]–[9]. However, one aspect of on-chip inductance that has not been well studied is mutual-inductive coupling. Mutual inductance causes signal-integrity issues by injecting noise pulses on a victim line. The injected noise can either cause functional failure or change the delay of the victim line [10]. Hence, it has become extremely important that accurate analytical-noise models be developed that include mutual inductance. These analytical models can then be used in signal-integrity-based physical-design optimizations.

Most existing noise models and avoidance techniques consider only capacitive coupling [11]–[13]. However, at current operating frequencies, inductive-crosstalk effects can be substantial and should be included for complete coupling-noise analysis. Fig. 1 shows noise waveforms for two fully coupled lines (in this case, minimum spacing is used along with a larger-than-minimum linewidth for *RC* delay reduction as may be done for critical global signals). The figure also shows waveforms for capacitive-coupling and inductive-coupling

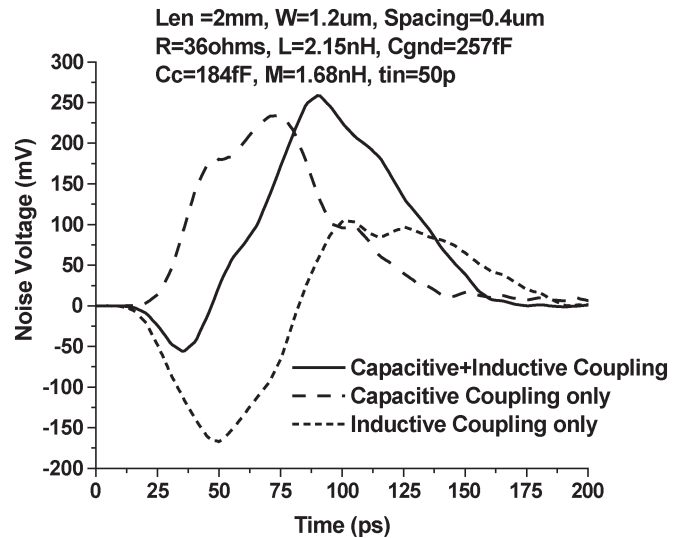


Fig. 1. Noise waveforms for capacitive, inductive, and capacitive + inductive coupling for two coupled lines.

noise separately.<sup>1</sup> The waveforms show that inductive noise can be comparable in magnitude to the noise due to capacitive coupling, and hence, neglecting inductance in noise analysis can be highly inaccurate.

Recently, there has been work incorporating inductive coupling into noise models. A noise model for two coupled *RLC* lines was proposed in [14]; however, this model is only applicable to loosely coupled lines for which mutual inductance and coupling capacitance are much smaller than self-inductance and ground capacitance, respectively. This approximation is not valid for on-chip interconnects where the ratio of coupling capacitance to ground capacitance can easily exceed one, and similarly, the ratio of mutual inductance to self-inductance can be in the range of 0.7 to 0.8 [15]. Another model for coupled *RLC* interconnects was proposed in [16]. The model maps two coupled lines to two isolated single lines and then approximates each isolated line as a one-segment *RLC* pi circuit. One disadvantage of this approach is that it applies only to identical wires with identical drivers. Furthermore, its use of a simple lumped one-segment pi approximation makes it invalid for fast transition times. At current frequencies, on-chip interconnects act as lossy transmission lines [17]. Hence, single-lump approximations for noise modeling are insufficient since transmission-line effects, such as time of flight and reflections, must be considered. Davis and Meindl [18] propose a model based on the rigorous solution of coupled distributed *RLC* lines, but the model is extremely complex and, as such, does not provide useful insight for physical-design noise optimizations.

In this paper, we propose a transmission-line-based coupling-noise model that is simple while retaining accuracy. In microwave applications, coupling in transmission lines has always been a problem and significant research has been done on this topic [19]–[23]. The proposed crosstalk-noise model is based on the transmission-line theory

Manuscript received July 6, 2004; revised December 13, 2004. This paper was recommended by Associate Editor F. N. Najm.

The authors are with the Department of Electrical Engineering and Computer Science, University of Michigan, Ann Arbor, MI 48109 USA.

Digital Object Identifier 10.1109/TCAD.2005.855961

<sup>1</sup>The capacitive-coupling-noise waveform is generated by setting the mutual inductance to zero, and similarly, inductive-coupling noise is generated by setting coupling capacitance to the ground capacitance. Note that the capacitive-coupling-noise waveform is not smooth due to the self-inductance of the line.

developed in these references. The transmission-line theory is applied to coupled on-chip interconnects under boundary conditions imposed by CMOS drivers and receivers. The model is then greatly simplified by making various key assumptions suitable for on-chip interconnects. Due to its simplicity, the model is useful in understanding noise waveform shapes due to capacitive and inductive coupling and also their dependencies on various parameters. The model can handle asymmetric line-and-driver configurations. The proposed model is then used in investigating the effect of physical-design changes (linewidth, spacing, shield insertion, etc.) on total (capacitive and inductive) noise. Results indicate that common (capacitive) noise-avoidance techniques can behave quite differently when both capacitive and inductive coupling are considered together.

The remainder of the paper is organized as follows. We begin by reviewing relevant transmission-line theory in the following section. The second section also presents our approach to modeling *RLC* coupling-noise waveforms. In Section III, we validate the new model by comparison to SPICE results. Using this model, we examine the effects of various physical-design optimizations on *RLC* noise in Section IV, before concluding in Section V.

## II. COUPLING-NOISE MODEL

In this section, we first review transmission-line theory for two coupled lines and then develop a new noise model based on this theory.

### A. Coupled-Transmission-Line Theory

This section reviews the basic concepts of coupled-transmission-line theory as proposed in various references [19]–[24]. Consider two distributed coupled *RLC* lines. Let  $R$ ,  $L$ , and  $C$  be the line resistance, self-inductance, and ground capacitance per unit length of the line, respectively. The lines are capacitively and inductively coupled. Let  $C_C$  be the per unit-length coupling capacitance and  $M$  be the per-unit-length mutual inductance between the lines. At any point  $z$  along the line, the voltage and current waveforms on line 1 and line 2 satisfy the following set of differential equations

$$\begin{aligned} -\frac{\partial V_1}{\partial z} &= (R + sL)I_1 - sMI_2 \\ -\frac{\partial V_2}{\partial z} &= (R + sL)I_2 - sMI_1 \\ -\frac{\partial I_1}{\partial z} &= s(C + C_C)V_1 - sC_C V_2 \\ -\frac{\partial I_2}{\partial z} &= s(C + C_C)V_2 - sC_C V_1. \end{aligned} \quad (1)$$

Here,  $V_1(z, t)$ ,  $I_1(z, t)$  and  $V_2(z, t)$ ,  $I_2(z, t)$  are voltage and current waveforms on lines 1 and 2, respectively. The generic solution of the above set of equations is given by

$$\begin{aligned} V_1 &= (A_1 e^{-\gamma_e z} + A_2 e^{\gamma_e z}) + (A_3 e^{-\gamma_o z} + A_4 e^{\gamma_o z}) \\ V_2 &= (A_1 e^{-\gamma_e z} + A_2 e^{\gamma_e z}) - (A_3 e^{-\gamma_o z} + A_4 e^{\gamma_o z}) \\ I_1 &= \frac{1}{Z_{0e}} (A_1 e^{-\gamma_e z} - A_2 e^{\gamma_e z}) + \frac{1}{Z_{0o}} (A_3 e^{-\gamma_o z} - A_4 e^{\gamma_o z}) \\ I_2 &= \frac{1}{Z_{0e}} (A_1 e^{-\gamma_e z} - A_2 e^{\gamma_e z}) - \frac{1}{Z_{0o}} (A_3 e^{-\gamma_o z} - A_4 e^{\gamma_o z}). \end{aligned} \quad (2)$$

Here, the  $A_i$ 's are constants whose values are obtained from the boundary conditions. The constants  $\gamma_e$  and  $\gamma_o$  are defined as even- and odd-mode propagation constants [24]. These constants are given by

$$\begin{aligned} \gamma_e &= \sqrt{sC [R + s(L + M)]} \\ \gamma_o &= \sqrt{s(C + 2C_C) [R + s(L - M)]}. \end{aligned} \quad (3)$$

Similarly,  $Z_{0e}$  and  $Z_{0o}$  are defined as even- and odd- mode characteristic impedances and can be expressed as

$$\begin{aligned} Z_{0e} &= \sqrt{\frac{R + s(L + M)}{sC}} \\ Z_{0o} &= \sqrt{\frac{R + s(L - M)}{s(C + 2C_C)}}. \end{aligned} \quad (4)$$

In the generic solution of (2),  $e^{-\gamma z}$  terms represent waves traveling in  $+z$  direction and  $e^{+\gamma z}$  terms represent waves traveling in  $-z$  direction. The first term  $A_1 e^{-\gamma_e z}$  in the expressions for  $V_1$  and  $V_2$  in (2) represents a voltage wave traveling in the  $+z$  direction with propagation constant  $\gamma_e$ , while the second term  $A_2 e^{\gamma_e z}$  represents the corresponding reflected wave traveling in the reverse direction. Similarly, the third and fourth terms represent similar traveling waves but with a different constant  $\gamma_o$ .

The above result clearly shows that coupled lines have two modes of propagation with two different propagation constants and two different characteristic line impedances. The interesting implication of this observation is that the solution of two coupled lines can be viewed as the combination of the solutions of two single-transmission lines. Physically, the even mode represents the case when both lines switch in the same direction and the odd mode represents the case when lines switch in opposite directions. Any signal traveling in the coupled-transmission-line system can be expressed as the superposition of these modes [25].

### B. Coupled-Noise Model

Based on the theory in Section II-A, an accurate coupling-noise model for on-chip interconnects can be developed. Fig. 2 shows two coupled interconnects where one line is switching and the other is quiet. The driver for the active line is replaced with a voltage ramp  $V_S$  in series with a Thevenin resistance  $R_S$ . For the quiet line, the driver is modeled as a linear resistance  $R_V$  connected to ground. Receivers at the far end of the lines are modeled as lumped capacitive loads.

For global interconnects in typical CMOS designs, the receiver has a small input capacitance (not more than few tens of femtofarads). At typical operating frequencies, this capacitive load at the far end of the line represents a large termination impedance ( $Z_L = 1/\omega C$ ) as compared to the characteristic impedance of the line. As a result, the far-end reflection coefficient in practical interconnects is around  $+1$  [26].<sup>2</sup> This implies that any forward-traveling wave is completely reflected at the far end and the voltage at the far-end of the line is doubled due to the superposition of the incident-voltage wave and the reflected reverse wave. In the generic solution given in (2), the

<sup>2</sup>The analysis can be extended to generic cases by considering a far-end reflection coefficient other than  $+1$ .

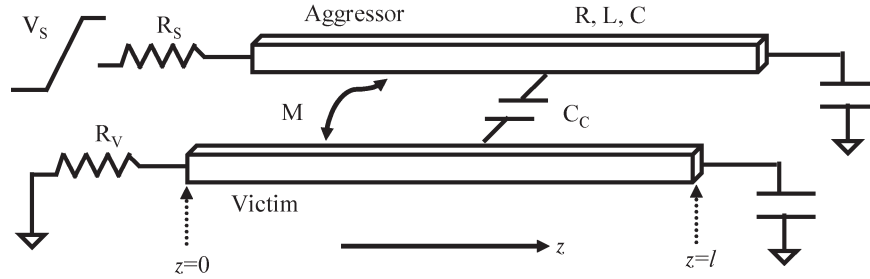


Fig. 2. Coupled-line configuration.

amplitude of the reflected wave can therefore be set equal to the incident wave and the solution of (2) can be simplified to

$$\begin{aligned} V_1 &= A_1(e^{-\gamma_e z} + e^{\gamma_e z}) + A_3(e^{-\gamma_o z} + e^{\gamma_o z}) \\ V_2 &= A_1(e^{-\gamma_e z} + e^{\gamma_e z}) - A_3(e^{-\gamma_o z} + e^{\gamma_o z}) \\ I_1 &= \frac{A_1}{Z_{0e}}(e^{-\gamma_e z} - e^{\gamma_e z}) + \frac{A_3}{Z_{0o}}(e^{-\gamma_o z} - e^{\gamma_o z}) \\ I_2 &= \frac{A_1}{Z_{0e}}(e^{-\gamma_e z} - e^{\gamma_e z}) - \frac{A_3}{Z_{0o}}(e^{-\gamma_o z} - e^{\gamma_o z}). \end{aligned} \quad (5)$$

At the near end ( $z = 0$ ), the active line (line 1) is driven by a voltage source  $V_S$  through a resistance  $R_S$  and the quiet line (line 2) is connected to ground through resistance  $R_V$ . Applying these boundary conditions to (5) gives

$$\begin{aligned} \frac{V_S - V_1(z=0)}{I_1(z=0)} &= \frac{V_S - (A_1 + A_3)}{\left(\frac{A_1}{Z_{0e}} + \frac{A_3}{Z_{0o}}\right)} = R_S \\ \frac{-V_2(z=0)}{I_2(z=0)} &= \frac{-(A_1 - A_3)}{\left(\frac{A_1}{Z_{0e}} - \frac{A_3}{Z_{0o}}\right)} = R_V. \end{aligned} \quad (6)$$

Solving the above set of equations for  $A_1$  and  $A_3$  gives

$$\begin{aligned} A_1 &= V_S \frac{Z_{0e}(Z_{0o} + R_V)}{(Z_{0e} + R_S)(Z_{0o} + R_V) + (Z_{0e} + R_V)(Z_{0o} + R_S)} \\ A_3 &= V_S \frac{Z_{0o}(Z_{0e} + R_V)}{(Z_{0e} + R_S)(Z_{0o} + R_V) + (Z_{0e} + R_V)(Z_{0o} + R_S)}. \end{aligned} \quad (7)$$

Now, let us first consider the case of lossless lines only. We will later consider losses in Section III. For lossless lines, the term  $e^{-\gamma_e z}$  in (5) simplifies to  $e^{-s(z\sqrt{C(L+M)})}$ . This simplified term in the  $s$ -domain corresponds to a time delay of  $z\sqrt{C(L+M)}$  in the time domain. Similarly, the exponential term for odd mode corresponds to a time delay of  $z\sqrt{(C+2C_C)(L-M)}$ . Hence, any voltage step generated at the near end in lossless coupled lines travels without any attenuation and distortion. For line length  $l$ , the step propagating with the even-mode constant arrives at the far end after an even time of flight  $t_{fe}$  and the step propagating with the odd-mode constant arrives at the far end after an odd time of flight delay  $t_{fo}$

$$\begin{aligned} t_{fe} &= l\sqrt{C(L+M)} \\ t_{fo} &= l\sqrt{(C+2C_C)(L-M)}. \end{aligned} \quad (8)$$

Based on the above theory, the far-end waveforms in coupled lossless lines can be computed by performing the following steps.

- 1) Given an input voltage ramp  $V_S(t)$ , compute the even and odd voltage ramps  $A_1(t)$  and  $A_3(t)$  using (7).
- 2) The voltage ramp  $A_1(t)$  arrives at the far end after  $t_{fe}$  and the voltage ramp  $A_3(t)$  arrives at the far end after a delay of  $t_{fo}$ .
- 3) Due to a reflection coefficient of  $+1$ , both the voltage ramps are doubled at the far end.
- 4) The far-end waveforms for active and quiet lines can be computed by superposition of the doubled voltage ramps. In the active line, both even and odd modes are positive, while in the quiet line, the even mode is positive, and the odd mode is negative.
- 5) Reverse traveling waves generated due to reflection at the far end travel back to the near end. Based on the mismatch between the characteristic line impedances and the source resistances, these waves can again get reflected at the near end and add to the far-end waveforms after three time-of-flight delays. Generally, these reflections are not significant and can be safely ignored.

The above flow is explained in Fig. 3. The figure shows that voltage steps  $A_1(t)$  and  $A_3(t)$  are generated at the near end of the lines. These steps travel with different velocities and arrive at the far end after different time delays. The output voltage waveforms can then be computed by

$$\begin{aligned} V_{agg}(t) &= 2A_1(t - t_{fe}) + 2A_3(t - t_{fo}) \\ V_{vic}(t) &= 2A_1(t - t_{fe}) - 2A_3(t - t_{fo}). \end{aligned} \quad (9)$$

Here,  $V_{agg}(t)$  and  $V_{vic}(t)$  are the waveforms at the output of aggressor and victim, respectively.

Now that we have discussed the theory of coupling noise, we seek to use the above concepts to analyze noise waveforms. Let us consider the case of inductive and capacitive coupling separately. The even- and odd-mode characteristic impedances and times of flight for capacitive and inductive coupling are given by the following expressions. For capacitive coupling only

$$\begin{aligned} t_{fe} &= l\sqrt{CL} & \text{and} & & Z_{0e} &= \sqrt{\frac{L}{C}} \\ t_{fo} &= l\sqrt{(C+2C_C)L} & & & Z_{0o} &= \sqrt{\frac{L}{(C+2C_C)}}. \end{aligned} \quad (10)$$

Similarly, for inductive coupling only

$$\begin{aligned} t_{fe} &= l\sqrt{C(L+M)} & \text{and} & & Z_{0e} &= \sqrt{\frac{(L+M)}{C}} \\ t_{fo} &= l\sqrt{C(L-M)} & & & Z_{0o} &= \sqrt{\frac{(L-M)}{C}}. \end{aligned} \quad (11)$$

Capacitive-coupling noise has positive polarity while inductive-coupling noise has negative polarity. This can be explained by the time-of-flight expressions in (10) and (11). For pure capacitive coupling, the even-mode time of flight is less than the odd-mode time of flight.

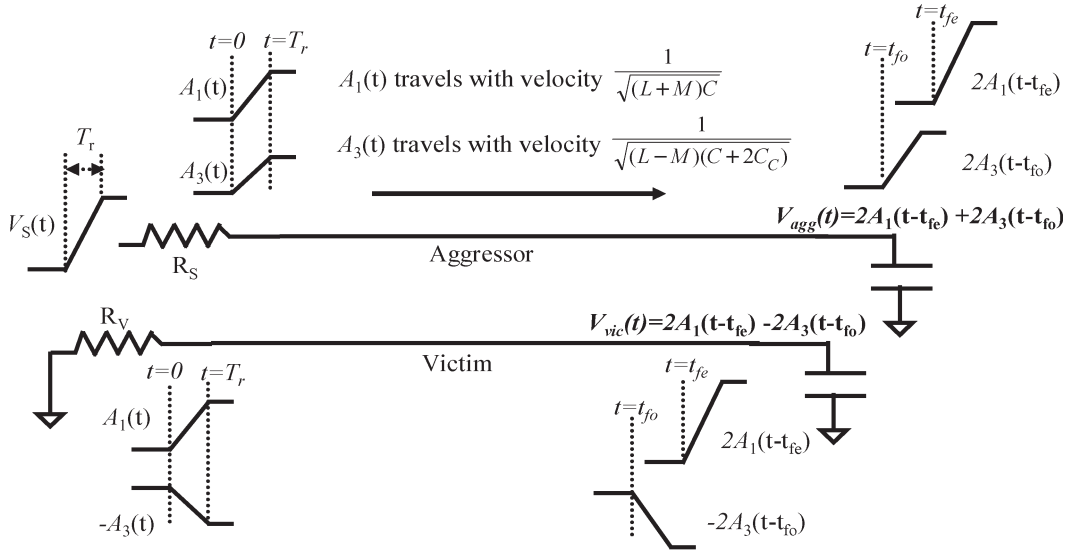


Fig. 3. Far-end waveform computation in coupled transmission lines.

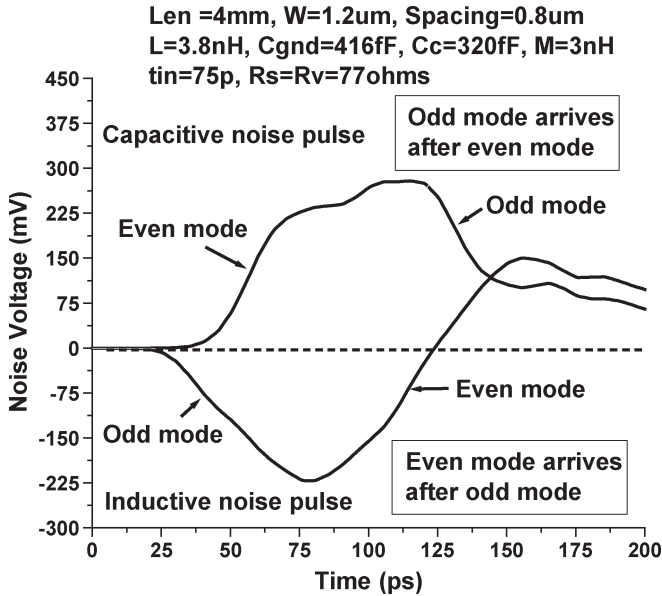


Fig. 4. Typical noise waveforms for capacitive- and inductive-coupling noise explained using even-odd-mode theory.

Hence, the even-mode voltage step arrives at the far end before the odd-mode step. Since even mode is positive and odd mode is negative, pure capacitive coupling results in a positive noise pulse. On the other hand, for pure inductive coupling, the negative odd-mode step travels faster than the positive even-mode step, thereby resulting in a negative-polarity noise pulse. Also, the even characteristic impedance is always larger than the odd characteristic impedance; thus the voltage step due to the even mode is bigger than the odd-mode step. These observations are summarized in Fig. 4 for capacitive- and inductive-noise waveforms in a 4-mm coupled pair of lines.

### C. Simultaneous Switching in Coupled RLC Interconnects

To this point, we have seen that coupled lines have two modes of propagation with two different propagation constants and two different characteristic line impedances. As mentioned in Section II-A, even mode represents the case when both lines switch in the same direction and odd mode represents the case when lines switch in opposite direc-

tions. All other scenarios including noise in the coupled transmission-line system can be expressed as a superposition of these modes. In general, coupled noise can be divided into two categories: 1) functional crosstalk noise in which a quiet line experiences a voltage spike due to an adjacent line switching; and 2) a change in signal-propagation delay when adjacent lines switch simultaneously either in phase or out of phase. Analyzing the simultaneous-switching case is equally important as modeling functional crosstalk noise, particularly since CMOS logic gates tend to have very good functional-noise rejection capabilities, whereas the second form of coupling noise impacts the critical issue of timing. In this work, we focus on coupling noise, but the simultaneous-switching scenario can be modeled in a similar manner. Due to its importance, we now briefly discuss the simultaneous-switching case and show that it can be easily modeled using our formulation.

Let us first consider the case when both aggressor and victim switch in the same direction and let us assume that the drivers for both the lines are replaced with a voltage ramp  $V_S$  in series with a Thevenin resistance  $R_S$ . We can now write the boundary conditions similar to (6). Solving these boundary conditions results in the odd voltage ramp  $A_3$  being zero, while the even voltage ramp  $A_1$  is given by

$$A_1 = V_S \frac{Z_{0e}}{(Z_{0e} + R_S)} \quad \text{where} \quad Z_{0e} = \sqrt{\frac{(L+M)}{C}}. \quad (12)$$

Similarly, for the opposite-switching case it can be shown that the even-mode voltage ramp  $A_1$  is zero, while the odd voltage ramp  $A_3$  is given by

$$A_3 = V_S \frac{Z_{0o}}{(Z_{0o} + R_S)} \quad \text{where} \quad Z_{0o} = \sqrt{\frac{(L-M)}{(C+2C_C)}}. \quad (13)$$

Equations (12) and (13) can be used to analyze simultaneous-switching scenarios in coupled RLC transmission lines. The most significant observation here is that, for simultaneous switching, the coupled-line system can be decoupled into single lines with new characteristic line impedances. The characteristic impedances depend on the switching polarities of aggressor and victim wires. If we consider only capacitive coupling, then the characteristic impedance for the in-phase (same direction)-switching case contains only ground capacitance and is independent of the coupling capacitance. On the other hand, for out-of-phase switching, there is an additional coupling capacitance ( $2 * C_C$ ) term along with the ground capacitance. This

result implies that, for capacitive coupling, the coupled lines can be decoupled into single lines with total capacitance equal to the ground capacitance  $C$  (for in-phase switching) or  $C + 2 * C_C$  (for out-of-phase switching). This result is identical to that obtained using a Miller effect-based analysis [27], where the coupling capacitance between two adjacent wires is replaced by a ground capacitance for each net. Traditional noise-aware static-timing analysis methodologies also set coupling capacitance to either 0 or  $2 * C_C$  for best and worst case analysis [28]–[30].

If we consider the impact of simultaneous switching on inductance, (12) and (13) suggest that for in-phase switching, the effective line inductance is given by  $L + M$ , while for out-of-phase switching, effective inductance of the decoupled single line reduces to  $L - M$ . Again, a similar observation has been made in some earlier works showing that the effective inductance of a line increases for in-phase switching and reduces for out-of-phase switching [31], [32]. Various design approaches have recently been developed to exploit differential-signaling switching to reduce inductive effects [33], [34]. All these works explain the impact of switching on inductance based on current return paths. However, most of these explanations are qualitative in nature and do not give any analytical formulation quantifying the impact of simultaneous switching on inductance. Based on the coupled-transmission-line theory discussed in this paper, not only can we get a physical understanding of this effect, but the proposed simplified models can also be used to quantify the impact of simultaneous switching on capacitively and inductively coupled on-chip interconnects.

#### D. Noise Model for Different Line Parasitics

Now we consider the case of two coupled lines with different line parasitics. The solution developed in this section is similar in nature as the even-odd mode solution for symmetric lines. The configuration considered is the same as in Fig. 2. The line parasitics per unit length for the active line (line 1) are  $R_1$ ,  $L_1$ , and  $C_1$ , and those for the quiet line are  $R_2$ ,  $L_2$ , and  $C_2$ . The differential equations in this case are given by

$$\begin{aligned} -\frac{\partial V_1}{\partial z} &= (R_1 + sL_1)I_1 + sMI_2 \\ -\frac{\partial V_2}{\partial z} &= (R_2 + sL_2)I_2 + sMI_1 \\ -\frac{\partial I_1}{\partial z} &= s(C_1 + C_C)V_1 - sC_C V_2 \\ -\frac{\partial I_2}{\partial z} &= s(C_2 + C_C)V_2 - sC_C V_1. \end{aligned} \quad (14)$$

The generic solution for this set of differential equations (considering a far-end reflection coefficient of +1) is given by

$$\begin{aligned} V_1 &= A_1(e^{-\gamma_e z} + e^{\gamma_e z}) + A_3(e^{-\gamma_o z} + e^{\gamma_o z}) \\ V_2 &= A_2(e^{-\gamma_e z} + e^{\gamma_e z}) + A_4(e^{-\gamma_o z} + e^{\gamma_o z}) \\ I_1 &= \frac{A_1}{Z_{0e1}}(e^{-\gamma_e z} - e^{\gamma_e z}) + \frac{A_3}{Z_{0o1}}(e^{-\gamma_o z} - e^{\gamma_o z}) \\ I_2 &= \frac{A_2}{Z_{0e2}}(e^{-\gamma_e z} - e^{\gamma_e z}) + \frac{A_4}{Z_{0o2}}(e^{-\gamma_o z} - e^{\gamma_o z}). \end{aligned} \quad (15)$$

For simplicity, let us consider the case of lossless lines (this assumption will be addressed in Section III). Even- and odd-mode propagation constants  $\gamma_e$  and  $\gamma_o$  are given by

$$\begin{aligned} \gamma_e &= s\sqrt{\frac{(a_1 + a_2) + \sqrt{(a_1 - a_2)^2 + 4b_1 b_2}}{2}} \\ \gamma_o &= s\sqrt{\frac{(a_1 + a_2) - \sqrt{(a_1 - a_2)^2 + 4b_1 b_2}}{2}} \end{aligned} \quad (16)$$

where

$$\begin{aligned} a_1 &= L_1(C_1 + C_C) - MC_C \\ b_1 &= -L_1 C_C + M(C_2 + C_C) \\ a_2 &= L_1(C_2 + C_C) - MC_C \\ b_2 &= -L_2 C_C + M(C_1 + C_C). \end{aligned} \quad (17)$$

For symmetric lines,  $a_1 = a_2 (= a)$  and  $b_1 = b_2 (= b)$ , and the expressions for even- and odd-mode propagation constants in (16) reduce to

$$\begin{aligned} \gamma_e &= s\sqrt{a + b} = s\sqrt{C(L + M)} \\ \gamma_o &= s\sqrt{a - b} = s\sqrt{(C + 2C_C)(L - M)}. \end{aligned} \quad (18)$$

In the solution of (15), the coefficients are related as

$$\begin{aligned} \frac{A_1}{A_2} &= \frac{(a_1 - a_2) + \sqrt{(a_1 - a_2)^2 + 4b_1 b_2}}{2b_2} \\ \frac{A_3}{A_4} &= \frac{(a_1 - a_2) - \sqrt{(a_1 - a_2)^2 + 4b_1 b_2}}{2b_2}. \end{aligned} \quad (19)$$

Again for symmetric lines,  $A_2 = A_1$  and  $A_4 = -A_3$ , and (15) properly reduces to the equation for symmetric lines. Another difference for asymmetric lines is that even- and odd-mode characteristic impedances for the two lines are different. These impedances are given by

$$\begin{aligned} Z_{0e1} &= \frac{s(L_1 L_2 - M^2)}{\gamma_e (L_2 - \frac{A_2}{A_1} M)} & Z_{0e2} &= \frac{s(L_1 L_2 - M^2)}{\gamma_e (L_2 - \frac{A_1}{A_2} M)} \\ Z_{0o1} &= \frac{s(L_1 L_2 - M^2)}{\gamma_o (L_2 - \frac{A_4}{A_3} M)} & Z_{0o2} &= \frac{s(L_1 L_2 - M^2)}{\gamma_o (L_2 - \frac{A_3}{A_4} M)}. \end{aligned} \quad (20)$$

Applying the boundary condition in a similar way as that for symmetric lines, the voltage steps traveling on the quiet line can be computed as

$$\begin{aligned} A_2 &= \frac{V_S}{\left(\frac{A_1}{A_2}\right)\left(\frac{Z_{0e1} + R_S}{Z_{0e1}}\right) - \left(\frac{A_3}{A_4}\right)\left(\frac{Z_{0e2} + R_V}{Z_{0e2}}\right)\left(\frac{Z_{0o2}}{Z_{0e2}}\right)\left(\frac{Z_{0o1} + R_S}{Z_{0o1}}\right)} \\ A_4 &= \frac{V_S}{\left(\frac{A_3}{A_4}\right)\left(\frac{Z_{0o1} + R_S}{Z_{0o1}}\right) - \left(\frac{A_1}{A_2}\right)\left(\frac{Z_{0o2} + R_V}{Z_{0e2} + R_V}\right)\left(\frac{Z_{0e2}}{Z_{0o2}}\right)\left(\frac{Z_{0e1} + R_S}{Z_{0e1}}\right)}. \end{aligned} \quad (21)$$

The overall flow for computing noise waveforms in asymmetric lines is the same as that in symmetric lines. For a given input ramp to the active line, the two voltage ramps  $A_2(t)$  and  $A_4(t)$  are generated on the quiet line. The two ramps propagate at different speeds and arrive at the far end of the line after  $t_{fe}$  and  $t_{fo}$  time of flights, respectively. These waveforms get doubled at the far end and the noise waveform is then computed by the superposition of these two ramps. The times of flight are given by

$$\begin{aligned} t_{fe} &= l\sqrt{\frac{(a_1 + a_2) + \sqrt{(a_1 - a_2)^2 + 4b_1 b_2}}{2}} \\ t_{fo} &= l\sqrt{\frac{(a_1 + a_2) - \sqrt{(a_1 - a_2)^2 + 4b_1 b_2}}{2}}. \end{aligned} \quad (22)$$

An analytical transmission-line-coupling model for different line parasitics was also proposed in [35]. However, the solution proposed in the reference is very different from our approach. In our methodology,

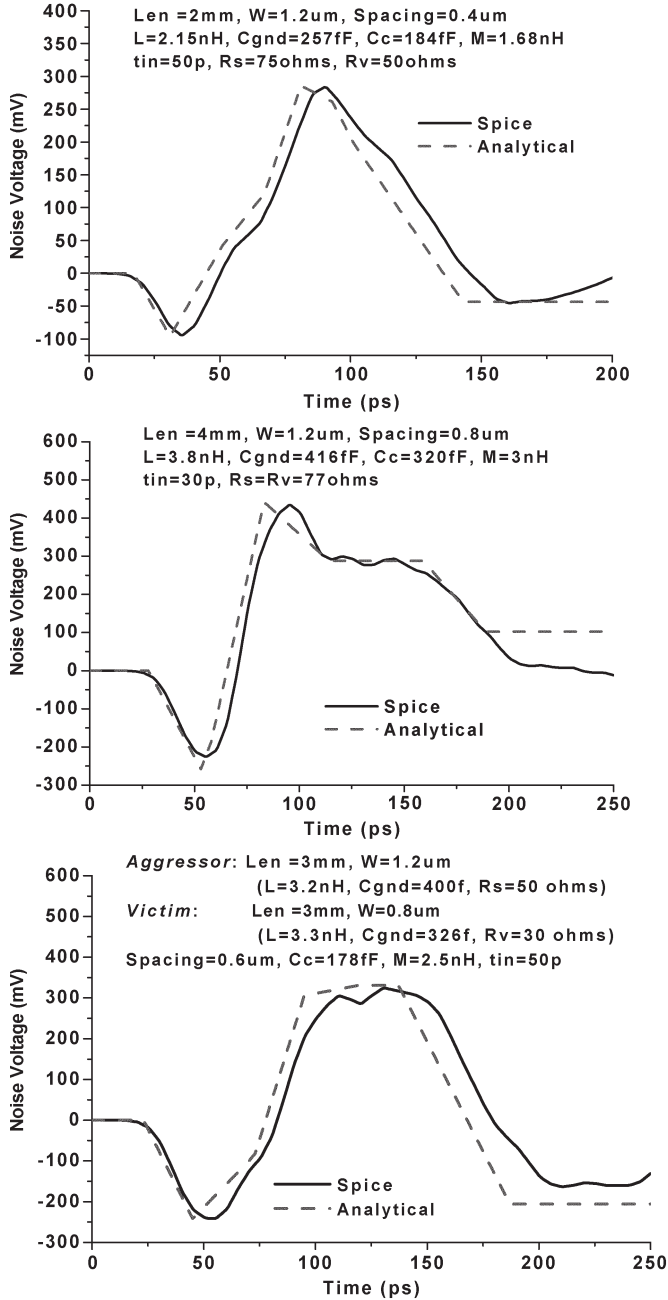


Fig. 5. Noise waveforms using SPICE and the analytical model.

we maintain the framework of even-odd mode approach used for symmetric lines. This allows us to keep the physical insight behind noise pulse shapes and their dependencies on design parameters. On the contrary, the solution proposed in the reference is based on the rigorous matrix manipulation and lacks the simplicity and the physicality inherent in our approach. In Section IV, we will investigate the effect of line parameters on coupling noise and show that the observed behavior can be explained by the proposed transmission-line model.

### III. VALIDATION OF THE MODEL

In this section, we test the previously developed model by comparing it to SPICE simulations. We consider a range of test cases with realistic interconnect topologies (for example, maximum interconnect length considered is 4 mm because wires longer than 4 mm are often broken into shorter wires by repeater insertion). Far-end

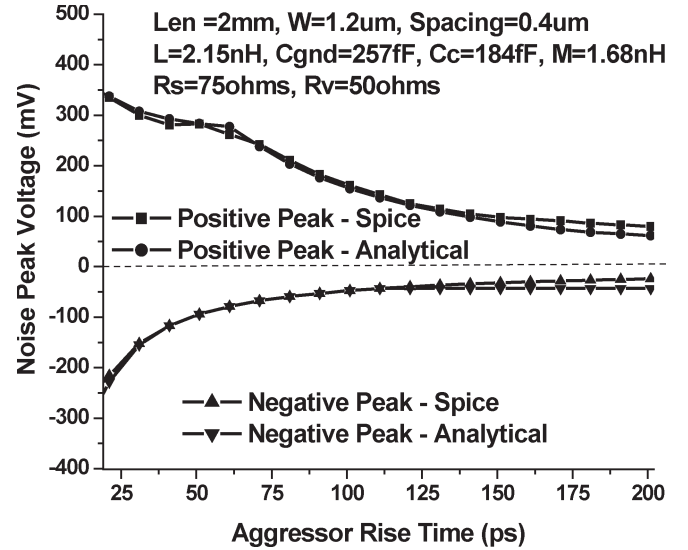


Fig. 6. Measured and calculated noise peak for various input aggressor transition time.

capacitive loading of 30 fF is considered in simulations. Line parasitics are extracted using the commercial extraction tool Raphael. A two-layer orthogonal power-grid structure with 50- $\mu\text{m}$  pitch and 10- $\mu\text{m}$  linewidth is used in the inductance extraction. All simulations use a 0.13- $\mu\text{m}$  1.2-V technology.

Fig. 5 shows the comparison between the model and SPICE for three arbitrarily chosen test cases. These test cases consider different aggressor and victim line configurations and driver strengths. In computing the model waveforms, the first set of reflections from the near end were also considered. The figure shows that the noise pulses have complicated waveforms due to mutual inductance and these waveforms are modeled well by the proposed analytical model. For one of these cases, we swept the aggressor input transition time from 20 to 200 ps. Fig. 6 compares the measured and calculated peak-noise values as a function of input transition time. The figure shows that the proposed model works well over a wide range of aggressor rise time typically observed in high-frequency interconnects. In all these test cases, line resistance was not considered.

Now, we discuss the effect of line resistance on noise waveforms. Fig. 7 shows SPICE waveforms for three different line resistances. The figure shows that as line resistance increases, the noise peak reduces. This is due to the fact that, with resistance, the voltage steps traveling along the line undergo attenuation and dispersion. Hence, the voltage steps arriving at the far end of the line are smaller and have larger rise times. This causes noise pulses in the lossy lines to be smaller and wider compared to those in a lossless line. This is helpful since the noise-peak values obtained using a lossless approximation can be safely assumed to be pessimistic.

Including resistance in the transmission-line analysis adds significant complexity to the problem and the resulting equations fail to provide much physical insight. For simplicity, a low-loss approximation is used to include the effect of line resistance in the above lossless model. In a low-loss approximation ( $R < 2Z_0$ ), a voltage step traveling along a transmission line of characteristic impedance  $Z_0$  is attenuated by a factor of  $e^{-R/2Z_0}$  [25]. Based on this theory, positive and negative noise-peak values in lossy lines can be computed as

$$\begin{aligned}
 V_{\text{lossy}}^- &= V_{\text{lossless}}^- \times e^{-\frac{R}{2Z_0}} \\
 V_{\text{lossy}}^+ &= V_{\text{lossless}}^- \times e^{-\frac{R}{2Z_0}} \\
 &\quad + (V_{\text{lossless}}^+ - V_{\text{lossless}}^-) \times e^{-\frac{R}{2Z_0}}. \quad (23)
 \end{aligned}$$



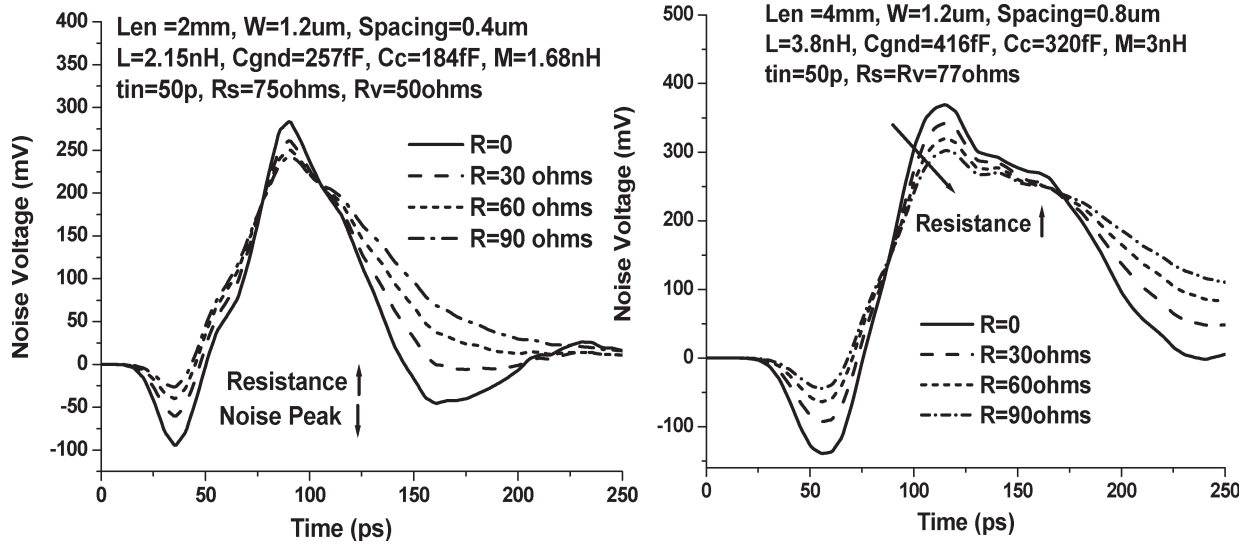


Fig. 7. Noise waveforms for three different line resistances.

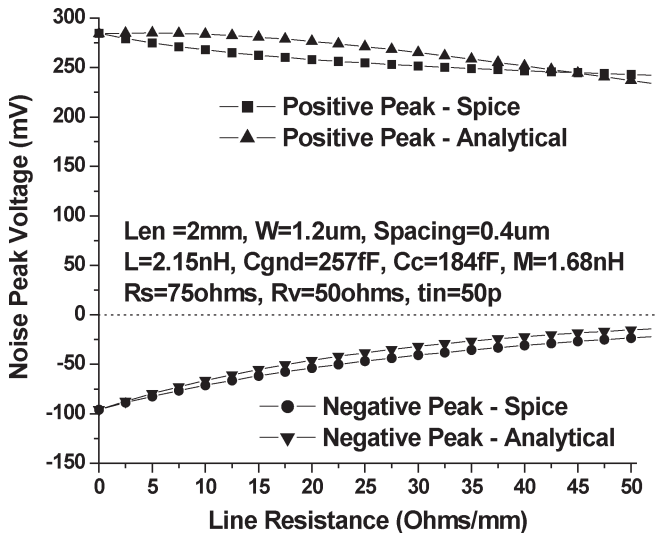


Fig. 8. Measured and calculated noise peak for various line resistances.

TABLE I  
ERROR BINS IN PEAK-NOISE ESTIMATION FOR 532 TEST CASES

Error bins	<5%	<10%	<15%
% of testcases	52%	81%	90%

Here,  $V^-$  and  $V^+$  represent the negative and positive peaks, respectively.

Fig. 8 shows SPICE and analytical results obtained by sweeping line resistance. The figure shows that both negative and positive noise peak decrease with line resistance, and this effect is captured well by the analytical equations.

Finally, we tested the complete analytical model including the lossy approximation by sweeping line length from 1 to 4 mm and linewidth from 0.8 to 3.2  $\mu\text{m}$ . Line-to-line spacing was swept from 0.4 to 1  $\mu\text{m}$ . We also varied input transition time from 50 to 150 ps. Table I shows the error bins in peak-noise estimation for these 532 test cases covering different wire topologies. The table shows that the model works very well with 81% of the test cases showing less than 10% error. The average error in noise-peak estimation over the entire set

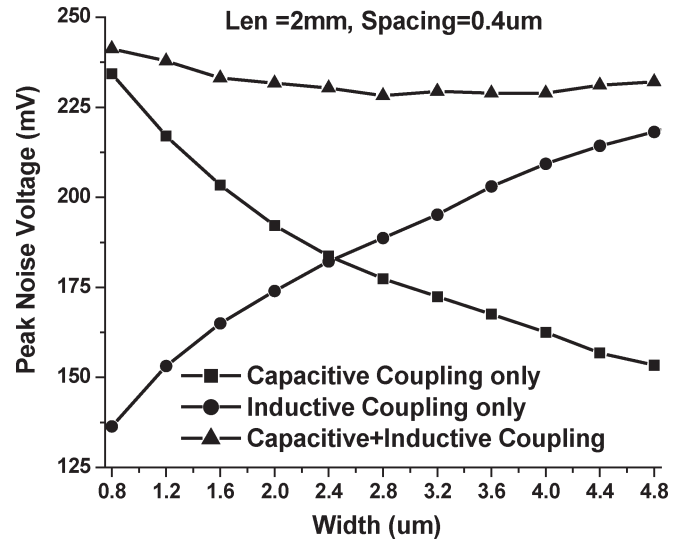


Fig. 9. Absolute peak-noise voltage versus linewidth for capacitive, inductive, and capacitive + inductive coupling.

of 532 test cases was 6.5%. On examining the test cases, we found that cases with large errors correspond to long and narrow wires. Such wires are not common in practical designs because they have high line resistance and hence are buffered more often to reduce  $RC$  delay. The primary source of error in such test cases is the low-loss approximation of (23). We also examined the extracted line parasitics in these 532 cases and found that only 7% of the test cases satisfy the loosely coupled approximation [ $(M/L) < 0.33$  and  $(C_C/C) < 0.33$ ] used in [14]. This indicates that the model proposed in [14] is not valid for practical on-chip interconnects; in particular, since coupling noise is by definition most problematic for tightly coupled wires and the model from [14] does not work in that regime. Similarly, we note that the model proposed in [16] assumes identical driver resistances and line configurations for aggressor and victim and, as such, cannot be applied to any large set of realistic test cases such as those used in this section.

#### IV. EFFECT OF LINE PARAMETERS ON COUPLING NOISE

The analytical noise model proposed in the previous sections can be used to quickly screen for logic (or timing) failures due to coupling

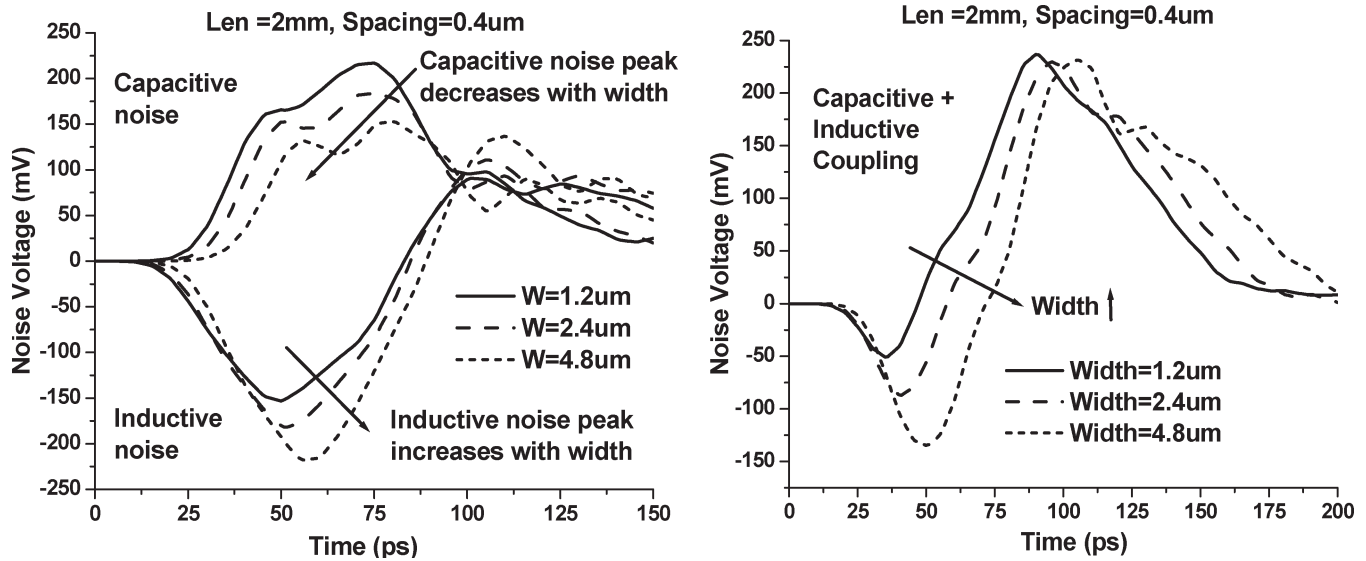


Fig. 10. Noise waveforms for capacitive and inductive coupling (left) and for capacitive + inductive coupling (right) for three different linewidths.

noise during physical design. Once a failure is detected, the routing should be modified to ensure proper operation. One way to manage coupling noise is by controlling line parasitics, which in turn can be controlled by wire sizing and spacing as well as shield line insertion. In this section, we study the effect of changing line parasitics on inductive and capacitive noise. Before we study these effects in detail, we highlight two observations from the theory discussed in Section II.

- 1) As the difference between even-mode and odd-mode times of flight increases, peak noise rises. This is due to the fact that even- and odd-mode voltage ramps are in the opposite direction. Hence, if the difference in their arrival times is larger, then the voltage step due to the first mode (mode that arrives first at the far end) can rise to a higher value before being pulled down by the second mode.
- 2) For a fixed victim driver resistance, the height of the even step increases as the ratio  $Z_{0e}/(Z_{0e} + R_S)$  increases. Similarly, the height of the odd step increases with a rise in the ratio  $Z_{0o}/(Z_{0o} + R_S)$ . This indicates that the ratio of aggressor driver resistance to characteristic line impedances plays an important part in controlling the noise.

A. Effect of Linewidth (Ground Capacitance) on Noise

For physical-design tools, linewidth is an important parameter during wire optimization because it has a significant effect on both line resistance and ground capacitance. In this section, we consider the effect of linewidth on coupling noise. We consider two coupled lines where each line is 2-mm long and the spacing between them is fixed at 0.4  $\mu\text{m}$ . Linewidth of both wires is swept from 0.8 to 4.8  $\mu\text{m}$  in steps of 0.4  $\mu\text{m}$ . For each width, line parasitics were extracted using the commercial extraction tool Raphael.

For each width, peak noise is computed using the model proposed in this paper. We consider three cases—capacitive coupling only, inductive coupling only, and the complete case where both forms of coupling are included. As linewidth increases, the ground capacitance of the line increases. With increased line capacitance, the aggressor transition time slows down considerably. Hence, for a fair comparison, the aggressor driver resistance was varied such that the RC product of driver resistance and total line capacitance remains constant. The input transition time to the aggressor is 50 ps, victim driver resistance is 50  $\Omega$ , and the aggressor driver resistance varies from 100 to

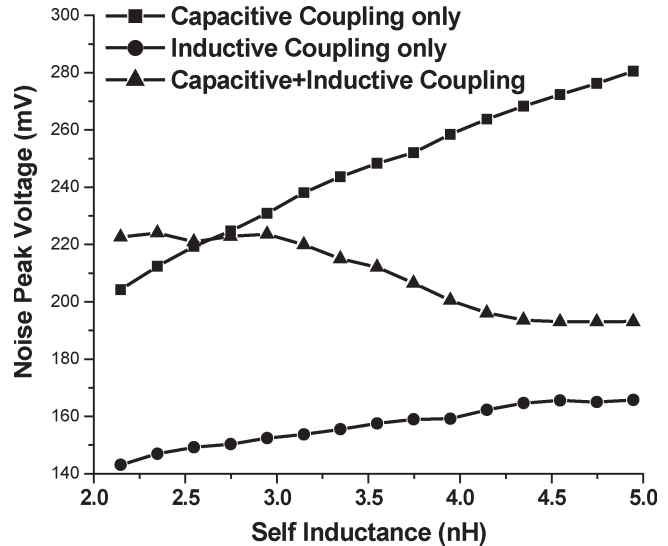


Fig. 11. Absolute peak-noise voltage versus line self-inductance for capacitive, inductive, and capacitive + inductive coupling.

42  $\Omega$ . Fig. 9 shows the absolute peak-noise voltage as a function of linewidth. The figure shows that as linewidth increases, noise peak due to capacitive coupling reduces as expected, while the noise peak due to inductive coupling increases. The actual noise peak while considering both forms of coupling is not very sensitive to the width. This is an interesting result since increasing linewidth is traditionally considered a useful noise-avoidance technique, although it actually worsens inductive noise. We also simulate the full noise waveforms for three different linewidths in SPICE. Fig. 10 shows the waveforms for capacitive, inductive, and both coupling cases for three different linewidths.

The above behavior of capacitive and inductive noise can be explained based on the theory discussed in the paper. For capacitive coupling, the even-mode time of flight is given by  $l\sqrt{LC}$  while the odd-mode time of flight is given by  $l\sqrt{L(C + 2C_C)}$ . Now, as ground capacitance  $C$  increases, the difference between even- and odd-mode times of flight reduces. This causes capacitive noise to reduce with width. For inductive coupling, the difference between even-mode time of flight ( $l\sqrt{(L + M)C}$ ) and the odd-mode time of



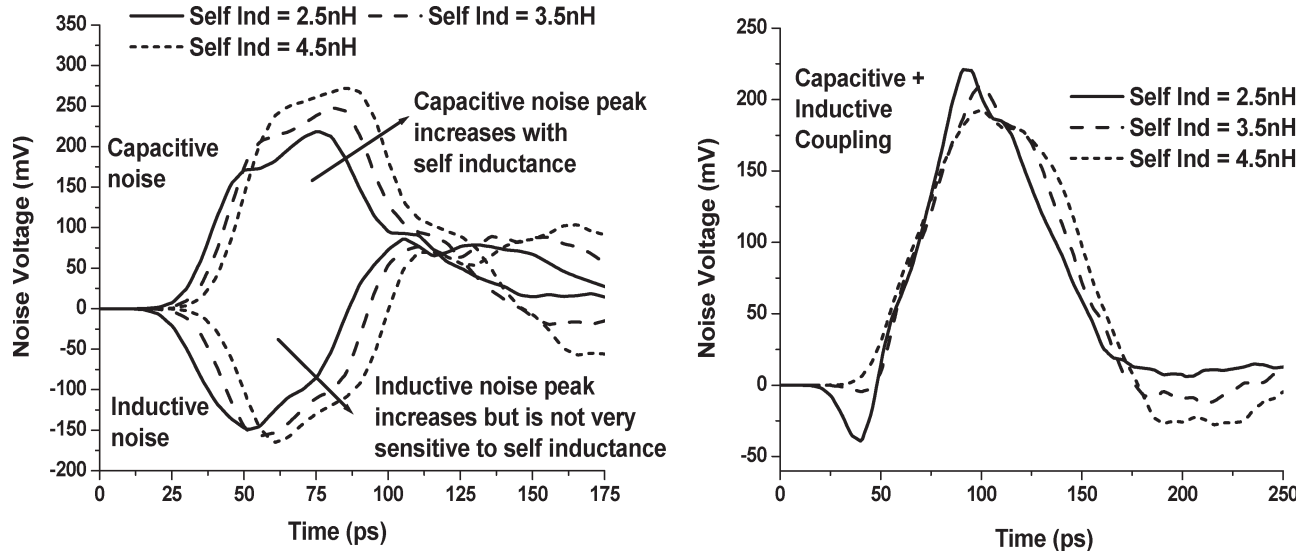


Fig. 12. Noise waveforms for capacitive and inductive coupling (left) and for capacitive + inductive coupling (right) for three different line self-inductances.

flight ( $l\sqrt{(L-M)C}$ ) increases with a rise in ground capacitance  $C$ . Hence, contrary to capacitive coupling, inductive-coupling noise peak increases with linewidth. It should be noted that with increased ground capacitance, both even and odd-mode characteristic impedances reduce. If driver resistance is fixed, then this results in reduced heights for even- and odd-mode steps. However, in our experiment, aggressor driver resistance was decreased to maintain a fixed  $RC$  product; making the effect of change in characteristic impedances on noise peak less significant.

### B. Effect of Self Inductance on Noise

Unlike capacitance, inductance is only a weak function of line geometry and is primarily controlled by the location of current return paths. With the increasing significance of inductance arising from technology scaling, it is required that physical-design tools consider inductance during shield insertion and power-grid specification. In this section, we study the effect of changing self-inductance on noise. Physically, self-inductance can be controlled by varying shield insertion and power-grid design during physical-design optimization. A similar setup as in Section IV-A is used. In the experiment, we consider 2-mm-long lines with 1.2- $\mu\text{m}$  width and 0.4- $\mu\text{m}$  spacing. Aggressor and victim driver resistances are 100 and 50  $\Omega$ , respectively, and input transition time is 50 ps. Instead of using extracted self-inductance values, it is swept from 2 to 5 nH.

Fig. 11 shows absolute peak-noise voltages as a function of self-inductance calculated using the model. The figure shows that as self-inductance increases, noise peak due to capacitive coupling increases significantly. Noise peaks while considering inductive coupling only as well as the total noise considering both couplings are not very sensitive to the width. This result is notable since it indicates that increasing self-inductance affects capacitive noise more than inductive noise. Also, consider that with capacitive coupling, when the ratio of coupling capacitance to ground capacitance is reduced, the capacitive noise reduces. Along the same lines for inductance, one might speculate that increasing the self-inductance should reduce the mutual-to-self-inductance ratio, and hence, reduce inductive noise. However, in our experiment, we found that for increasing self-inductance, the noise peak due to inductive coupling increases slightly. Fig. 12 shows SPICE waveforms for capacitive, inductive, and total coupling cases for three different self-inductances.

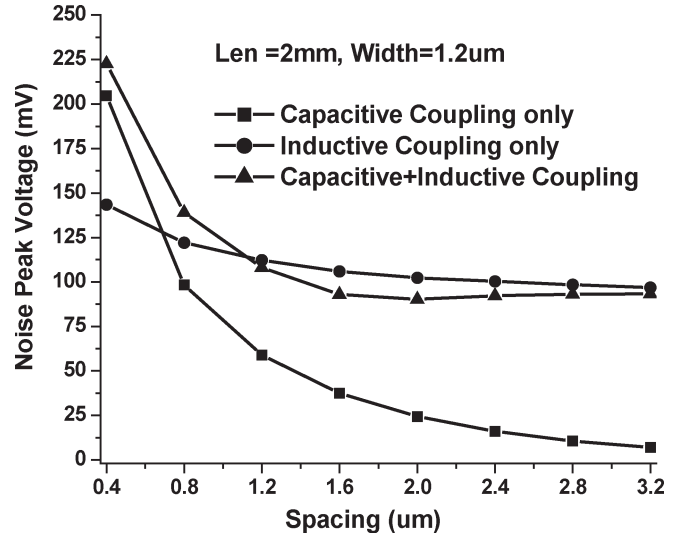


Fig. 13. Absolute peak-noise voltage versus line-to-line spacing for capacitive, inductive, and capacitive + inductive coupling.

This behavior can again be explained by the two observations made in the beginning of this section. For capacitive noise, as self-inductance is increased, the difference between even- ( $l\sqrt{LC}$ ) and odd-mode times of flight ( $l\sqrt{L(C+2C_c)}$ ) increases. Also, with self-inductance, the even- and odd-mode characteristic impedances also increase, causing capacitive noise to rise significantly. For inductive noise, the difference between even-mode time of flight ( $l\sqrt{(L+M)C}$ ) and the odd-mode time of flight ( $l\sqrt{(L-M)C}$ ) reduces, but characteristic impedances increase. Due to the conflicting impact of these two factors on noise, the inductive-noise peak is fairly insensitive to self-inductance.

### C. Effect of Spacing on Noise

Finally, we study the effect of spacing on noise. A similar setup as in Section IV-A is used. Line-to-line spacing is swept from 0.4 to 3.2  $\mu\text{m}$  in steps of 0.4  $\mu\text{m}$ . For each spacing, line parasitics are extracted and coupling-noise behavior is computed using the newly

proposed *RLC* model. Fig. 13 shows the absolute peak-noise voltages as a function of spacing. The figure shows that with increased spacing, noise peaks due to both capacitive and inductive coupling reduce. As expected, the reduction in inductive noise is not as significant as that in the capacitive noise. This is due to the fact that with spacing, the coupling capacitance reduces more rapidly as compared to the mutual inductance. The figure also shows that for large spacings, the total noise is dominated by inductive coupling only. This implies that only small increases in spacing are useful (e.g., in this case, from 0.4 to 0.8  $\mu\text{m}$ ), since beyond this point, noise reductions saturate due to the presence of mutual inductance.

## V. CONCLUSION

In this paper, we proposed a simple crosstalk-noise model for coupled on-chip interconnects. The main contribution of this work is analyzing the impact of mutual inductive coupling on crosstalk noise. The proposed model is based on coupled-transmission-line theory and is applicable to asymmetric driver-and-line configurations. Our results show that the model captures the noise-waveform shape well and yields an average error of 6.5% for noise peak over a wide range of test cases. The proposed model is not only useful for accurate noise estimation in the presence of inductive effects, but it can also be very effective in guiding noise-aware physical-design optimizations. To illustrate this point, the model is used to investigate sensitivities of total (capacitive + inductive) noise to layout parameters such as width, spacing, and power-grid granularity. Our analysis shows that in the presence of mutual inductance, crosstalk noise behaves very differently as compared to the noise behavior under purely capacitive coupling. This leads us to conclude that traditional capacitive-coupling-based physical-design noise optimizations are not always effective when both capacitive and inductive coupling are considered together, and new layout guidelines must be developed for effective reduction of crosstalk noise in coupled *RLC* wires.

## REFERENCES

- [1] Y. I. Ismail and E. G. Friedman, *On-Chip Inductance in High Speed Integrated Circuits*. Norwell, MA: Kluwer, 2001.
- [2] C. K. Cheng, J. Lillis, S. Lin, and N. Chang, *Interconnect Analysis and Synthesis*. New York: Wiley, 2000.
- [3] A. Deutsch *et al.*, "When are transmission line effects important for on-chip interconnections?" *IEEE Trans. Microw. Theory Tech.*, vol. 45, no. 10, pp. 1836–1846, Oct. 1997.
- [4] M. H. Chowdhury, Y. I. Ismail, C. V. Kashyap, and B. L. Krauter, "Performance analysis of deep sub micron VLSI circuits in the presence of self and mutual inductance," in *Proc. IEEE Int. Symp. Circuits and Systems*, Scottsdale, AZ, 2002, pp. 197–200.
- [5] R. Arunachalam, F. Dartu, and L. T. Pileggi, "CMOS gate delay models for general RLC loading," in *Proc. Int. Conf. Computer Design*, Austin, TX, 1997, pp. 224–229.
- [6] K. Agarwal, D. Sylvester, and D. Blaauw, "A library compatible driving point model for on-chip RLC transmission lines," *IEEE Trans. Comput.-Aided Des. Integr. Circuits Syst.*, vol. 23, no. 1, pp. 128–136, Jan. 2004.
- [7] A. Kahng and S. Muddu, "An analytical delay model for RLC interconnects," *IEEE Trans. Comput.-Aided Des. Integr. Circuits Syst.*, vol. 16, no. 12, pp. 1507–1514, Dec. 1997.
- [8] Y. I. Ismail, E. G. Friedman, and J. L. Neves, "Equivalent Elmore delay for RLC trees," *IEEE Trans. Comput.-Aided Des. Integr. Circuits Syst.*, vol. 19, no. 1, pp. 83–97, Jan. 2000.
- [9] Y. Lu, M. Celik, T. Young, and L. T. Pileggi, "Min/max on-chip inductance models and delay metrics," in *Proc. Design Automation Conf.*, Las Vegas, NV, 2001, pp. 341–346.
- [10] A. Deutsch *et al.*, "The importance of inductance and inductive coupling for on-chip wiring," in *Proc. Topical Meeting Electrical Performance Electrical Packaging*, San Jose, CA, 1997, pp. 53–56.
- [11] D. Sylvester and K. Shepard, "Electrical integrity design and verification for digital and mixed-signal systems on a chip," in *Tutorial—Int. Conf. Computer Aided Design*, San Jose, CA, Nov. 2001.
- [12] A. Vittal, L. Chen, M. Marek-Sadowska, K. P. Wang, and S. Yang, "Crosstalk in VLSI interconnections," *IEEE Trans. Comput.-Aided Des. Integr. Circuits Syst.*, vol. 18, no. 2, pp. 1817–1824, Dec. 1999.
- [13] K. L. Shepard and V. Narayanan, "Noise in deep submicron digital design," in *Proc. Int. Conf. Computer-Aided Design*, San Jose, CA, 1996, pp. 524–531.
- [14] K. T. Tang and E. G. Friedman, "Interconnect coupling noise in CMOS VLSI circuits," in *Proc. Int. Symp. Physical Design*, Monterey, CA, 1999, pp. 48–53.
- [15] L. He, N. Chang, S. Lin, and O. S. Nakagawa, "An efficient inductance modeling for on-chip interconnects," in *Proc. Custom Integrated Circuits Conf.*, San Diego, CA, 1999, pp. 457–460.
- [16] L. Yin and L. He, "An efficient analytical model of coupled on-chip RLC interconnects," in *Proc. Asia South Pacific Design Automation Conf.*, Yokohama, Japan, 2001, pp. 385–390.
- [17] K. Banerjee and A. Mehrotra, "Analysis of on-chip inductance effects for distributed RLC interconnects," *IEEE Trans. Comput.-Aided Des. Integr. Circuits Syst.*, vol. 21, no. 8, pp. 904–915, Aug. 2002.
- [18] J. Davis and J. Meindl, "Compact distributed RLC interconnect models—Part II: Coupled line transient expressions and peak crosstalk in multilevel networks," *IEEE Trans. Electron Devices*, vol. 47, no. 11, pp. 2078–2087, Nov. 2000.
- [19] H. R. Kaupp, "Pulse crosstalk between microstrip transmission lines," in *Proc. Int. Electronic Circuit Packaging Symp.*, San Jose, CA, Aug. 1966, vol. 2/5, pp. 1–12.
- [20] N. C. Arvanitakis, J. T. Koliass, and W. Radzelovage, "Coupled noise prediction in printed circuit boards for a high-speed computer system," in *Proc. Int. Electronic Circuit Packaging Symp.*, San Jose, CA, Aug. 1966, vol. 2/6, pp. 1–11.
- [21] I. Catt, "Crosstalk (noise) in digital systems," *IEEE Trans. Electron. Comput.*, vol. EC-16, no. 6, pp. 743–763, Dec. 1967.
- [22] A. Feller, H. R. Kaupp, and J. J. DiGiacomo, "Crosstalk and reflections in high-speed digital systems," in *Proc. Fall Joint Computer Conf.*, Anaheim, CA, 1965, pp. 511–525.
- [23] J. B. Connolly, "Cross coupling in high speed digital systems," *IEEE Trans. Electron. Comput.*, vol. EC-15, no. 3, pp. 323–327, Jun. 1966.
- [24] K. C. Gupta, *Microstrip Lines and Slotlines*. Norwood, MA: Artech House, 1996.
- [25] H. B. Bakoglu, *Circuits, Interconnections, and Packaging for VLSI*. Reading, MA: Addison-Wesley, 1990.
- [26] B. Young, *Digital Signal Integrity*. Englewood Cliffs, NJ: Prentice-Hall, 2001.
- [27] A. S. Sedra and K. C. Smith, *Microelectronic Circuits*. Fort Worth, TX: Saunders, 1991.
- [28] R. Arunachalam, K. Rajagopal, and L. T. Pileggi, "TACO: Timing Analysis with Coupling," in *Proc. Design Automation Conf.*, Los Angeles, CA, 2000, pp. 266–269.
- [29] P. F. Tehrani, S. W. Chyou, and U. Ekambaram, "Deep submicron static timing analysis in presence of crosstalk," in *Int. Symp. Quality Electronic Design*, San Jose, CA, 2000, pp. 505–512.
- [30] B. Franzini, C. Forzan, D. Pandini, P. Scandolaro, and A. Dal Fabbro, "Crosstalk aware static timing analysis: A two step approach," in *Proc. Int. Symp. Quality Electronic Design*, San Jose, CA, 2000, pp. 499–503.
- [31] P. Restle, A. Ruehli, and S. Walker, "Dealing with inductance in high-speed chip design," in *Proc. Design Automation Conf.*, New Orleans, LA, 1999, pp. 904–909.
- [32] Y. Cao, X. Huang, N. Chang, S. Lin, O. S. Nakagawa, W. Xie, D. Sylvester, and C. Hu, "Effective on-chip inductance modeling for multiple signal lines and application on repeater insertion," *IEEE Trans. Very Large Scale Integr. (VLSI) Syst.*, vol. 10, no. 6, pp. 799–805, Dec. 2002.
- [33] Y. Massoud, J. Kawa, D. Macmillan, and J. White, "Modeling and analysis of differential signaling for minimizing inductive crosstalk," in *Proc. Design Automation Conf.*, Las Vegas, NV, 2001, pp. 804–809.
- [34] H. Kaul, D. Sylvester, and D. Blaauw, "Clock net optimization using active shielding," in *Proc. Eur. Solid State Circuits*, Lisbon, Portugal, 2003, pp. 265–268.
- [35] C. R. Paul, *Analysis of Multiconductor Transmission Lines*. New York: Wiley, 1994.